Proceedings of A S M E FEDSM'00
ASME 2000 Fluids Engineering Division Summer Meeting
June 11-15, 2000, Boston, MA, USA

FEDSM2000-11145

A NUMERICAL INVESTIGATION OF UNSTEADY BUBBLY CAVITATING NOZZLE FLOWS

Al Preston*
Tim Colonius
Christopher E. Brennen

Division of Engineering and Applied Science
California Institute of Technology
Pasadena, CA 91125
email: alastair@its.caltech.edu

ABSTRACT

The effects of unsteady bubble dynamics on cavitating flow through a converging-diverging nozzle are investigated numerically. A continuum model that couples the Rayleigh-Plesset equation with the continuity and momentum equations is used to formulate unsteady, quasi-one-dimensional partial differential equations. These equations are solved numerically using a Lagrangian finite volume method. Special formulations are used at the boundary cells to allow Eulerian boundary conditions to be specified. Flow regimes studied include those where steady state solutions exist, and those where steady state solutions diverge at the so-called *flashing instability*. These latter flows consist of unsteady bubbly shock waves travelling downstream in the diverging section of the nozzle. The computations show reasonable agreement with an experiment that measures the spatial variation of pressure, velocity and void fraction for steady shockfree flows, and good agreement with an experiment that measures the shock position and throat pressure for flows with bubbly shocks.

INTRODUCTION

The first model of two phase flow through a converging-diverging nozzle was proposed by Tangren et al. (1949). They employed a barotropic relation, which assumes that the fluid pressure is a function of fluid density only. This implies that the only effect of the disperse gas phase is to allow fluid compressibilty which results in the bubbly mixture being treated as a single-phase compressible fluid. Brennen (1995) provides a general discussion of these barotropic models, as well as a summary of the work of Tangren et al..

Bubble dynamics are neglected by the barotropic models, but are thought to significantly alter the flow in cavitating nozzles, even in the mean. Wang & Brennen (1998) applied a nonlinear continuum bubbly mixture model to the computation of the steady flow through a converging-diverging nozzle. This model was first proposed by van Wijngaarden (1968, 1972) and incorporates the Rayleigh-Plesset equation to predict bubble size and growth as a function of position and time. Wang & Brennen found two different steady state flow regimes to exist, and termed them *quasi-steady* and *quasi-unsteady*. The former is characterized by bubble growth that is induced by the low pressure region in the nozzle contraction, followed by a series of bubble collapses and rebounds downstream of the contraction. The quasi-unsteady solutions correspond to *flashing* flow. Varying the upstream conditions causes the flow to bifurcate from one regime to the other. The bifurcation of the steady equations has been studied in detail by Delale et al. (1998).

To illustrate the two regimes, the method of Wang & Brennen is applied to a nozzle with a gentle contraction, depicted in Fig. 1. Wang & Brennen investigated the bifurcation by varying the inlet void fraction; here we vary the cavition number,

* Address all correspondence to this author.

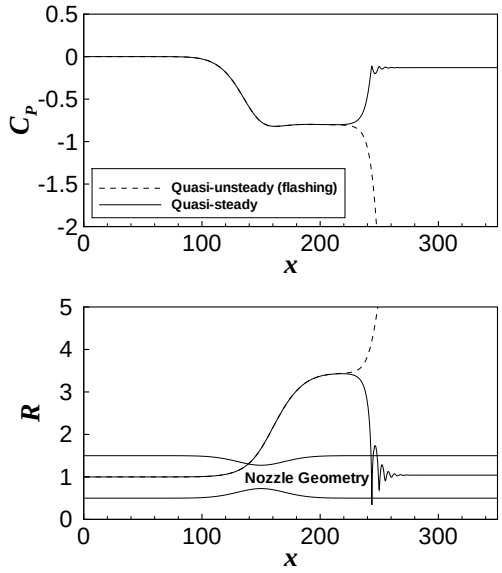

Figure 1. The pressure coefficient and bubble radius for two steady computations. Solid line is *quasi-steady* ($\sigma = \sigma^{+}_{crit}$), dashed line is *quasi-unsteady* or *flashing* ($\sigma = \sigma^{-}_{crit}$). Other parameters are, $\alpha_0 = 10^{-2}$, $We = 117$, $\delta_D = 0.43$.

σ, and achieve a similar transition. Figure 1 presents the computed steady state solutions for the pressure and bubble radius for cavitation numbers either side of the critical bifurcation value. The solid and dashed lines correspond respectively to the quasi-steady and quasi-unsteady solutions.

It is apparent in Fig. 1 that the flashing solution has unbounded bubble growth which results in a physically unrealistic downstream pressure. Physically realizable steady-state solutions do not exist in this flow regime, and hence an *unsteady* code is required to examine these flows. Ishii et al. (1993) proposed an unsteady bubbly flow model for the study of flows through a convergent-divergent nozzle. However, by assuming that the pressure inside the bubbles is equal to the ambient fluid presure, they neglected the bubble dynamics which are important in the cavitating nozzle flow. The present work employs an unsteady quasi-one-dimensional code, based on the bubbly flow model used by Wang & Brennen, to demonstrate that the physically correct solutions in the flashing regime involve *unsteady* bubbly shock waves propagating downstream from the nozzle contraction.

THE MODEL AND NUMERICAL METHOD

We consider a homogeneous[1] continuum bubbly mixture model that was first proposed by van Wijngaarden (1968, 1972). The model starts with the conventional quasi-one-dimensional continuity and momentum equations for flow of a compressible fluid through a nozzle:

$$\frac{\partial}{\partial t}(\rho A) + \frac{\partial}{\partial x}(\rho u A) = 0, \tag{1}$$

$$\rho \frac{Du}{Dt} + \frac{1}{2}\frac{\partial C_P}{\partial x} = 0. \tag{2}$$

Note that the viscous terms and gravity have been neglected in the momentum equation. The two-phase bubbly mixture is now assumed to be made up of an incompressible liquid phase with a dilute gas phase consisting of many spherical bubbles. By assuming that the flow properties vary on length scales that are large compared to the bubble radius and noting that the gas phase is restricted to being dilute we can, at any point in the flow, relate the local bubble radius to the local pressure by the Rayleigh-Plesset equation:

$$\begin{aligned} R\frac{D^2R}{Dt^2} + \frac{3}{2}\left(\frac{DR}{Dt}\right)^2 + \delta_D \frac{1}{R}\frac{DR}{Dt} \\ + \frac{2}{We}\left[R^{-1} - R^{-3k}\right] \\ + \frac{\sigma}{2}\left[1 - R^{-3k}\right] + \frac{C_P}{2} = 0. \end{aligned} \tag{3}$$

The bubble population per unit liquid volume is fixed (neither fission nor fusion occur), so that the following relation between the mixture density and bubble radius holds,

$$\rho = \left[1 + \frac{\alpha_0 R^3}{1-\alpha_0}\right]^{-1}, \tag{4}$$

where α_0 is the initial volume void fraction. Equations (3) and (4) dynamically relate the mixture density to the mixture pressure. These two equations effectively replace the usual barotropic relation used for single phase flows, and allow the set of equations to be closed.

In equations (1) to (4) ρ is the mixture density made dimensionless by the constant liquid density, ρ^d_L. The length and velocity scales used for non-dimensionalization are the equilibrium bubble radius, R^d_0, and the nozzle inlet velocity, u^d_0. The pressure coefficient is defined as $C_P = (p^d - p^d_0)/\frac{1}{2}\rho^d_L u^{d^2}_0$, where p^d_0 is the upstream pressure. The cavitation number is defined as $\sigma = (p^d_0 - p^d_v)/\frac{1}{2}\rho^d_L u^{d^2}_0$, where p^d_v is the vapor pressure of the liquid. The Weber number is given by $We = \rho^d_L R^d_0 u^{d^2}_0 / S^d$, where S^d is the (constant) surface tension. The polytropic index, k, is

[1] Applying an order of magnitude analysis (Brennen 1995) indicates that, for the present nozzle flows, relative motion of the two phases can be neglected.

either unity for isothermal flow, or the ratio of the specific heats of the gas phase for adiabatic flow. The *effective damping* for the radial motion of the spherical bubbles is denoted by δ_D and is discussed later in more detail. The nozzle area, A, is nondimensionalized by the inlet area, A_0^d. Since viscous terms are neglected, A_0^d does not appear as a parameter of the computation; only the axial area variation of the nozzle is relevent. Parenthetically, for comparisons to real experimental nozzles it is required that $\sqrt{A_{min}^d} \gg R_{max}^d$ for the continuum approximation to hold.

Equations (1) through (4) are integrated using a one-dimensional Lagrangian finite volume scheme. This formulation allows the substantial derivatives to be treated as ordinary derivatives, and hence the Rayleigh-Plesset equation can be integrated as an ordinary differential equation. Consider a quasi-one-dimensional nozzle divided longitudinally into $N-1$ control volumes. Denoting the position of the control volume faces as x_j ($j = 1,2,\ldots,N$), we can define the nozzle areas and their derivatives at these positions:

$$A_j = A(x_j), \tag{5}$$

$$A'_j = \frac{dA}{dx}(x_j), \tag{6}$$

where $A(x)$ and $dA(x)/dx$ are known functions. Each control volume face moves at the local fluid velocity and therefore:

$$\frac{dx_j}{dt} = u_j, \tag{7}$$

where u_j is shorthand for $u(x_j(t),t)$. Integrating equations (1) and (2) over the control volumes we obtain, for $j = 1,2,\ldots,N-1$:

$$\frac{d}{dt}\int_{x_j}^{x_{j+1}} \rho A dx = 0, \tag{8}$$

$$2\frac{d}{dt}\int_{x_j}^{x_{j+1}} \rho u A dx = A_j C_{P_j} - A_{j+1} C_{P_{j+1}} + \int_{x_j}^{x_{j+1}} C_P A' dx. \tag{9}$$

Equations (8) and (9) respectively describe the rate of change of the total mass and momentum in the j^{th} control volume. Also, Eq. (3) can be split into two first order equations at each face ($j = 1,2\ldots,N$):

$$\frac{dR_j V_j}{dt} + G_j + \frac{C_{P_j}}{2} = 0, \tag{10}$$

$$\frac{dR_j}{dt} - V_j = 0, \tag{11}$$

where,

$$G_j = \frac{V_j^2}{2} + \delta_D \frac{V_j}{R_j} + \frac{2}{We}\left[R_j^{-1} - R_j^{-3k}\right] + \frac{\sigma}{2}\left[1 - R_j^{-3k}\right]. \tag{12}$$

Finally, the density and bubble radius at the faces are related by:

$$\rho_j = \left[1 + \frac{\alpha_0 R_j^3}{1-\alpha_0}\right]^{-1}. \tag{13}$$

To integrate this system of (as yet exact) equations, it remains to approximate the integrals in equations (8) and (9). A second-order approximation is used:

$$\int_{x_j}^{x_{j+1}} f dx = \frac{\Delta x_j}{2}(f_j + f_{j+1}) + O(\Delta^3), \tag{14}$$

where $\Delta x_j \equiv x_{j+1} - x_j$, and f is any of ρA, $\rho u A$, or $C_P A'$.

Equations (5) to (13) are $8N-2$ ODEs for $8N$ unknowns ($\rho_j, R_j, V_j, C_{P_j}, u_j, A_j, A'_j$, and x_j at the edges of the control volumes, $j = 1,2,\ldots,N$). Specifying both of the boundary pressures, C_{P_1} and C_{P_N} closes the system. Alternative boundary conditions, such as the non-reflective boundary condition developed by Colonius et al. (1998, 1999), have also been successfully implemented. All results presented in this paper have the pressure specified at both boundaries.

The equations are solved in the Lagrangian coordinate system, whereas the nozzle boundary conditions should be implemented in an Eulerian coordinate system. To circumvent this situation a special control volume with a fixed upstream face and a moving downstream face is used at the upstream boundary. Hence we replace Eq. (7) for the $j = 1$ case with $x_1 =$ constant. Additional flux terms are also added to equations (8) through (11). It is clear that the control volume will become very large as the downstream face is convected away from the stationary upstream face. Remeshing is required to ensure that the accuracy of Eq. (14) is maintained. This is achieved by simply splitting the control volume into two as necessary as the computation proceeds. Maintaining consistency with the order of approximation of Eq. (14), variable values at the new face are obtained by linearly interpolating from values at either side. As a new control volume is created at the upstream boundary a control volume is removed from the downstream boundary. Hence the downstream boundary is only approximately fixed in position, with fluctuations caused by the truncations as well as net expansions or compressions of the fluid over the entire domain.

In practice the downstream boundary is positioned far enough from the nozzle contraction that, after initial transients, there are no appreciable gradients in the solution near the boundary, so that the exact location of the boundary is not important.

The discretized equations have similar properties to those arising in earlier work (Colonius et al. 1998, 1999) that examined the generation of bubbly shocks by an oscillating plane boundary. That is, they are stiff, and do not conserve mass precisely when an explicit time marching scheme is used. Hence an implicit Euler method is used for the basic time advancement. This is combined with a Richardson extrapolation method of which the details are given by Hairer & Wanner (1996). The basic premise of the method is to compute a series of predictions for the solution at the new time level based on different numbers of subdivisions of the time interval. The series of predictions is then used to extrapolate to the limit of zero time step, and to provide an error estimate for the integration. The overall time step is adjusted based on the number of subdivisions and the error estimate. Colonius et al. (1998, 1999) demonstrated through numerical experiments that this scheme was far more efficient than first and second order implicit schemes. Given the similarity of their equations to the present equations, we would expect the same to hold here.

The basic time advancement of the extrapolation method is the implicit Euler method. For an ODE given by:

$$\frac{df}{dt} = f', \tag{15}$$

the discrete form is:

$$f^{n+1} = f^n + h f'^{n+1}, \tag{16}$$

where h is the time step. Using this integration scheme on equations (7) to (11) and going through the algebra, we can establish $2N$ equations of the form:

$$F_j(X_k^{n+1}) = 0, \qquad j = 1,\ldots,2N, \qquad k = 1,\ldots,2N, \tag{17}$$

where $\vec{X} \equiv [u_1, R_1, x_2, R_2, x_3, R_3, \ldots, x_N, R_N]$ is a vector containing the $2N$ unknowns. In each equation F_j, various parameters of the problem also appear as well as the fields from previous time levels. Newton's method is used to solve the nonlinear equations. When combined with the extrapolation scheme it is found that only one Newton iteration per time step is the most efficient, though in that case discrete global conservation is not guaranteed. The system of equations (17) results in a six-banded Jacobian matrix, enabling relatively efficient solution.

RESULTS

The nondimensional parameters that are chosen to be studied are $\alpha_0 = 10^{-2}$, $We = 117$, $\delta_D = 0.43$, $k = 1.4$ (adiabatic) and σ ranging from 0.93 to 1.20. The value of δ_D is chosen to achieve realistic solutions with only a few bubble rebounds. It is shown later that for an effective damping less than about 0.5 the macroscopic flow properties are independent of the effective damping. The nozzle has a Gaussian area variation given by,

$$A(x) = 1 - (1 - A_{min}) e^{-(\frac{x-x_0}{w})^2}, \tag{18}$$

and for the present study we focus on the values $A_{min} = 0.75$, $x_0 = 150.0$, $w = 30.0$.

Flow Regimes

A series of computations are performed where the back pressure is varied over a wide range. The computed pressure, bubble radius and flow velocity for a typical set of computations are presented in Fig. 2. The solid lines represent final steady state solutions (obtained by computing until steady state is reached), while the dashed lines represent instantaneous flowfields as an unsteady shock wave travels downstream through the nozzle.

It is seen that much like the quasi-one-dimensional nozzle flows for a perfect gas, different regimes exist depending upon the value of the back pressure. These regimes are,

(i) Steady solution with no shocks ($0 > C_{Pb} > C_{Pcrit_1}$)
For small negative back pressures there exist steady state solutions. One such solution is plotted as curve (i) in Fig. 2. It is apparent that there is only small growth of the bubble radius, and no collapses and rebounds. The small pressure gradient is supported by losses due to the effective damping term in the Rayleigh-Plesset equation.

(ii) Stationary shock in diverging section of nozzle ($C_{Pcrit_1} > C_{Pb} > C_{Pcrit_2}$)
The pressure drop is now large enough to cause choking at the throat and the formation of a steady bubbly shock wave in the diverging section of the nozzle. Curve (ii) represents one such solution. The bubbly shock structure is most apparent in the graph of the bubble radius, which shows the characteristic bubble growth followed by a succession of collapses and rebounds. The pressure in this case also exhibits a relatively sharp recovery associated with the bubbly shock wave.

(iii) Unsteady shock travelling down nozzle ($C_{Pcrit_2} > C_{Pb} \gtrsim -\sigma$)
The pressure drop is now large enough to cause the bubbly shock wave to move out of the diverging section and propagate downstream. The dashed curves of Fig. 2 show the solution at four different times. The time interval between

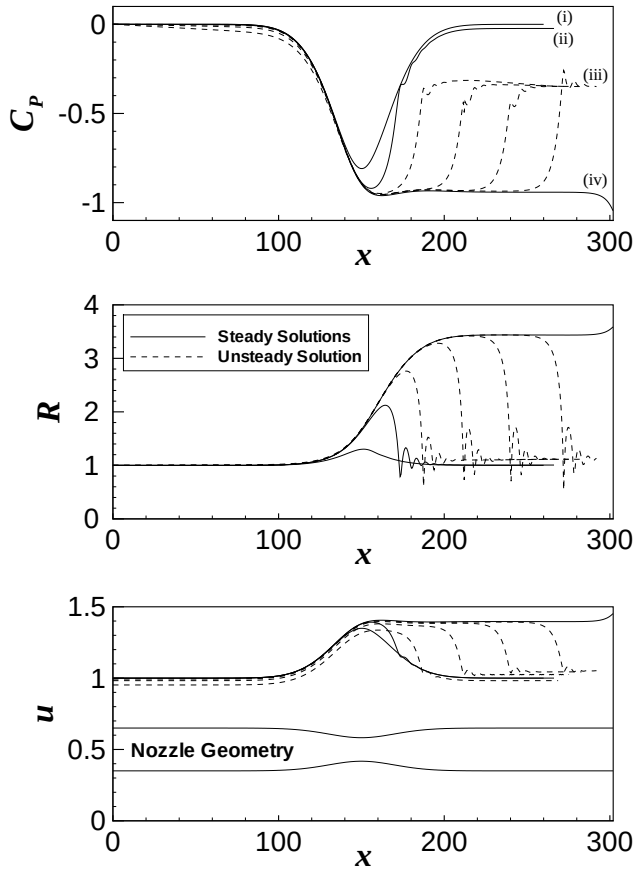

Figure 2. The pressure coefficient, bubble radius and flow velocity for four different back pressures. (i) Steady state solution with no shocks, (ii) Shock standing in diverging section of nozzle, (iii) Unsteady shock travelling downstream, (iv) Steady state solution with expansion near nozzle exit. (All computations have $\alpha_0 = 10^{-2}$, $We = 117$, $\delta_D = 0.43$, and σ ranges from 0.93 to 1.20.)

each curve is constant, so it is evident that the propagation speed of the bubbly shock is approximately constant. It is likely that within this range of back pressures it is physically possible to have a final *steady state* solution where the flow in the nozzle is "overexpanded", and the increase to the back pressure takes place across a system of bubbly shock waves outside the nozzle.

(iv) Steady, underexpanded flow ($C_{Pb} \lesssim -\sigma$)
Now the back pressure is low enough to allow the shock to pass through the downstream boundary and out of the computational domain. The flow in the nozzle is "underexpanded" and expands near the end of the nozzle to match the back pressure. This is apparent in curve (iv) of the pressure plot in Fig. 2, which shows the expansion taking place near the domain boundary.

Calculations with lower initial void fractions yielded behavior that was qualitatively identical to the higher void fraction computations. As expected, the lower void fraction results in higher maximum bubble radius and hence more violent collapses.

Choking

For small negative back pressures a steady state, shockfree solution exists. As the back pressure is lowered, the mass flow rate will increase until the flow eventually chokes and the mass flow rate becomes constant. To illustrate this phenomena many calculations of the steady flow solution were carried out to produce the curves in Fig. 3, which presents the mass flow rate (nondimensionalized by the choked mass flow rate) versus the back pressure. Results with effective dampings ranging from 0.22 to 0.85 are shown.

For very small negative back pressures the curves have a constant slope, which smoothly transition to choked flow (where the curves have no slope) as the negative back pressure is increased. It is interesting to note that the variation of effective damping does not affect the value of critical choking back pressure. The only significant impact that the value of effective damping has, is to cause the constant slope portion of the curve to shift sideways. This corresponds to the expected result that, for a given back pressure, cases with a smaller effective damping have a larger mass flowrate.

Figure 4 presents the bubble radius for four different back pressures indicated by (i)-(iv) in Fig. 3. Curve (i) in Fig. 4 illustrates that for small negative back pressures there are no bubble collapses or rebounds. This accounts for the straight sections of the curves in Fig. 3. For larger pressure drops bubble collapses and rebounds become apparent (curve (ii) in Fig. 4). This increases the losses in the system and hence causes the curved sections in Fig. 3. This smooth transition to choked flow continues as the negative back pressure becomes larger and the bubble dynamics become more pronounced (curve (iii) in Fig. 4), until eventually the flow chokes and a bubbly shock wave forms (curve (iv) in Fig. 4).

Effect of Damping

The appropriate magnitude of the effective damping, δ_D, which should be used in the Rayleigh-Plesset equation is an unresolved issue. van Wijngaarden (1972) reviews some analytical and empirical expressions for contributions to the effective damping from viscous, acoustic and thermal effects. These estimates are generally based on low amplitude motions, such as the attenuation of sound waves, whereas in the nozzle flow there is strong bubble growth and collapse. Comparisons between experiments and calculations show that for strong bubble collapses the value of effective damping required to achieve a realistic number of collapses and rebounds is far greater than those estimates

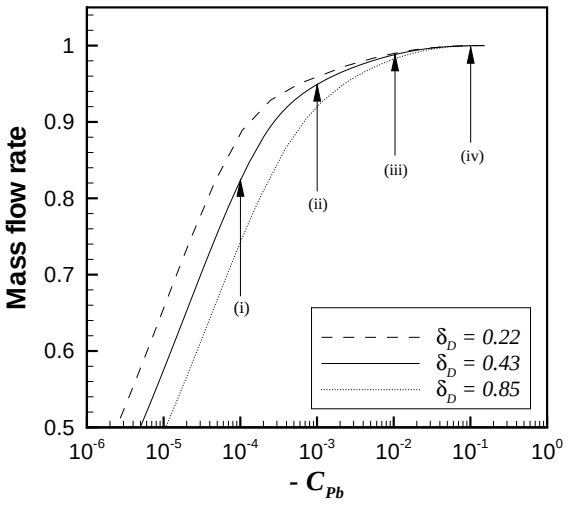

Figure 3. Non-dimensional mass flow rate as a function of back pressure for different values of effective damping, δ_D, in the range 0.22 to 0.85.

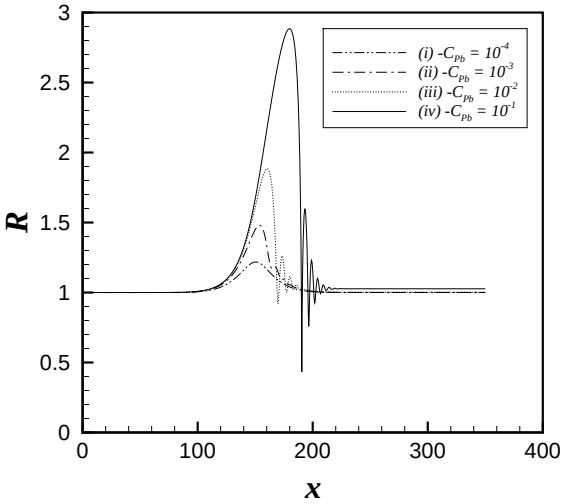

Figure 4. The bubble radii corresponding to the four back pressures indicated in Fig. 3.

given in van Wijngaarden. It seems likely that the bubble break up that occurs in real collapses would introduce additional and perhaps dominant damping mechanisms.

While we cannot fully explain these effects in the context of the present model, it is of interest to quantify the effect of the effective damping on the computed flow field. A series of unsteady computations with effective damping ranging from 0.22 to 3.78 was performed. The initial values of the other parameters

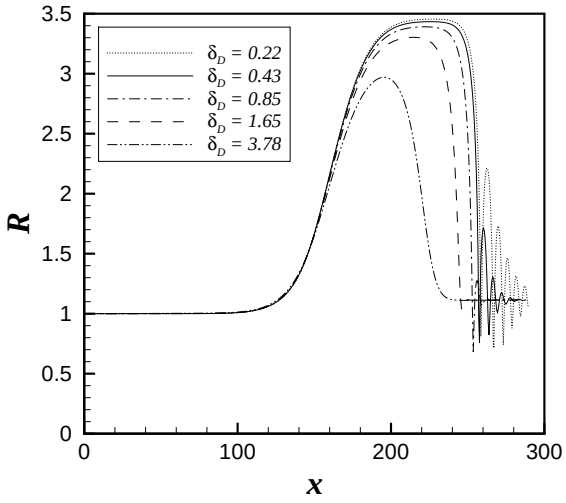

Figure 5. Bubble radius for a series of different values of effective damping, δ_D, in the range 0.22 to 3.78 ($\sigma = 0.76$ to 0.95, $-C_{P_b} = 0.27$ to 0.36, $We = 115$ to 153).

were held constant, but the final values of the parameters varied slightly due to the renormalization with the inlet velocity. Figure 5 plots the bubble radius for each of these calculations at a time when the bubbly shock is propagating in the constant area section of the nozzle. For values of effective damping lower than about 0.5 the macroscopic behavior is relatively independent of effective damping. That is, there is large growth of the bubble radius followed by a rapid collapse; the jump conditions across the shock are not significantly impacted by the value of effective damping. The main effect of decreasing the effective damping is to increase the amplitude and number of the bubble rebounds. For larger values of effective damping the bubble growth begins to be affected, eventually limiting the growth to the extent that there is no sharp collapse. These results are consistent with earlier work (Colonius et al. 1998, 1999) which examined the generation of bubbly shock waves by an oscillating plane boundary.

COMPARISON TO EXPERIMENTS

Shockfree steady flow

Here we will compare the results of the bubbly model with the experiments of Ishii et al. (1993) who measured the pressure, void fraction, and flow velocities of both the liquid and gas components at four locations in a steady nozzle flow, and compared them with their own bubbly flow model. Their model assumed that the pressure inside a bubble was equal to the ambient pressure, and hence neglected any of the bubble dynamics described by the Rayleigh-Plesset equation. They did however account for relative motion between the liquid and gas phases, which may be

important to correctly predict the void fraction distribution in the nozzle.

Non-dimensionalization of the flow parameters yields a cavitation number, $\sigma = 23.5$ and Weber number, $We = 20.7$. From the air and water mass flow rates that are provided, and assuming no relative motion at the inlet, it is possible to compute the inlet void fraction as, $\alpha_0 = 0.039$.

Since the experimental data is only for a steady run, a steady code based on that of Wang & Brennen (1998) is used to compute the solution. In addition the barotropic solution is calculated. Figure 6 shows the comparisons of the present dynamic computation (solid lines) and the barotropic calculation (dashed lines) to the experimentally measured pressures, void fractions and velocities of Ishii et al.. The maximum bubble growth in this flow is only about 7 percent which results in $\sqrt{A^d_{min}}/R^d_{max} = 124$, so the continuum approximation is valid. The small amount of bubble growth implies that bubble dynamics are not important for this flow. This accounts for the barotropic computation being almost identical to the dynamic computation. For flows nearing the critical regime, bubble dynamics become important and the dynamic and barotropic models obtain vastly different results.

Agreement of both the dynamic and barotropic models to the experimental pressure and liquid velocities is excellent, as it also was for the model of Ishii et al.. The computed void fraction fares much worse. The only point of agreement is right in the throat itself, with the other points being considerably lower upstream of the throat and higher downstream of the throat. The considerably more complicated model of Ishii et al., which incorporates the relative motion of the phases, had reasonable success at matching the first and last experimental points, but significantly underestimated the void fraction at and immediately downstream of the throat.

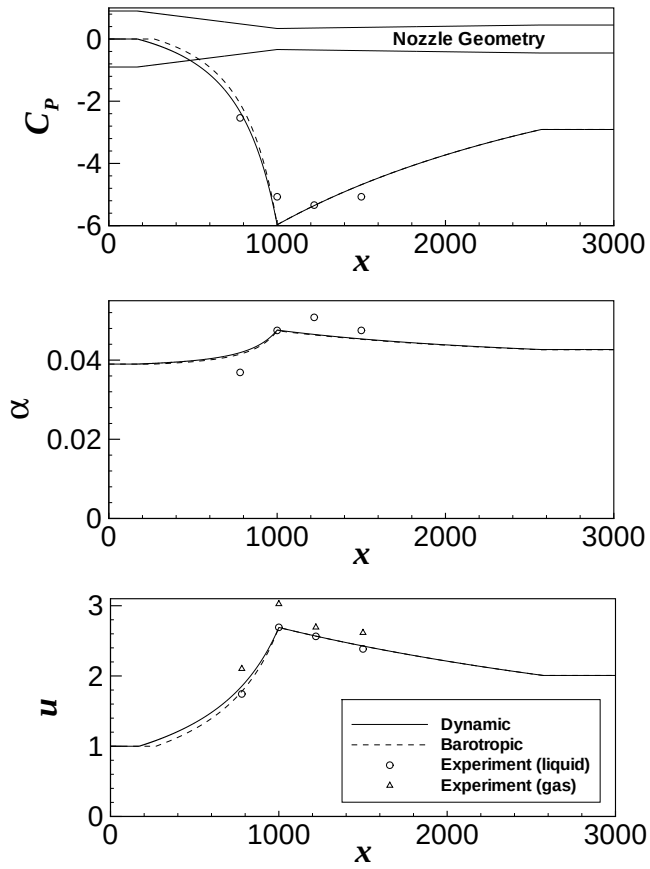

Figure 6. Comparison of Ishii et al.'s experimentally measured pressures, void fractions and velocities with dynamic and barotropic solutions ($\alpha_0 = 0.039, \sigma = 23.5, We = 20.7, \delta_D = 0.5$).

Unsteady flows with shocks

Sandhu & Jameson (1979) performed experiments in a converging diverging nozzle with equal inlet and outlet areas, and a throat area ratio of 0.132. Non-dimensionalization of the flow parameters yields a cavitation number of, $\sigma = 81.6$ and a Weber number, $We = 4.1$. The initial void fraction was $\alpha_0 = 0.107$. In calculations we use an effective damping of $\delta_D = 15.2$. Steady calculations similar to those presented in Fig. 5 determined this to be close to the upper limit, below which the value of δ_D does not have any significant impact on the maximum bubble growth and the jump conditions across the bubbly shock. The effective damping was chosen to be as close as possible to this limit to enable efficient computation, while still ensuring that its value did not impact the relevant flow physics.

Computations with different back pressures were performed. In each case as the back pressure was lowered the flow accelerated until at some instance the flow became choked and a bubbly shock wave formed in the diverging section of the nozzle. The position of the shock would oscillate about its steady state position for a few cycles. Computations were carried out until it was clear where the final steady state position of the shock was.

For these flows the maximum bubble growth was over 300 percent which results in $\sqrt{A^d_{min}}/R^d_{max} = 20$. The continuum approximation is probably still valid, but it should be noted that the dilute gas phase assumption is violated with void fractions as high as 25 percent being reached. Hence bubble-bubble interactions are important, and the Rayleigh-Plesset equation should be modified to account for this. Nevertheless, Fig. 7 shows remarkable agreement of the computed steady state shock position to the experimental observations presented in Fig. 4 of Sandhu & Jameson (1979). The slight rightward shift of the computed points can be attributed to the friction losses in the experiment that are not accounted for in the model. To end up with a bubbly shock in a certain fixed position, the experiment would require a larger negative back pressure to overcome the additional frictional losses. The computed throat pressures were also compared

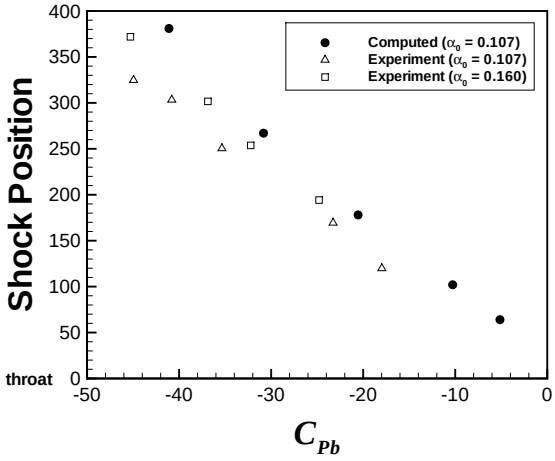

Figure 7. Shock position as a function of back pressure for present computation and experimental observations of Sandhu et al. (Parameters are, $\sigma = 81.6, We = 4.1, \delta_D = 15.2$.)

to those measured in the experiments and were found to be about ten percent larger. This can also be attributed to the neglect of friction losses in the model.

CONCLUSION

An efficient and accurate numerical method has been developed for computing unsteady, quasi-one-dimensional, bubbly cavitating flows through converging-diverging nozzles. Four different flow regimes are shown to exist depending on the value of the back pressure. For small negative back pressures there exist steady state solutions with no shocks. As the back pressure is lowered the flow becomes choked, and a steady bubbly shock wave forms in the diverging section of the nozzle. For lower back pressures the bubbly shock wave begins to travel downstream in the diverging section of the nozzle. This unsteady bubbly shock wave is the correct solution in the regime where steady state computations result in *flashing* solutions. Finally, for even lower back pressures, there exist underexpanded, steady state solutions with no shocks.

The computations show reasonable agreement with two sets of experiments; one where spatial variations of flow variables are measured in steady flows, and the other where shock position and throat pressure are measured for flows with bubbly shocks.

REFERENCES

Anderson, John, D. (1990), *Modern Compressible Flow: With Historical Perspective*, 2nd edn, McGraw-Hill.

Biesheuvel, A. & van Wijngaarden, L. (1984), 'Two phase flow equations for a dilute dispersion of gas bubbles in liquid', *Journal of Fluid Mechanics* **148**, 301–318.

Brennen, C. E. (1995), *Cavitation and Bubble Dynamics*, Oxford University Press.

Brennen, C. E., Colonius, T. & d'Auria, F. (1998*a*), Computing shock waves in cloud cavitation, Third International Symposium on Cavitation.

Brennen, C. E., Colonius, T., Wang, Y. C. & Preston, A. (1998*b*), 'Cloud cavitation phenomena', *Presented at the 22nd Symposium on Naval Hydrodynamics* pp. 1–15.

Colonius, T., Brennen, C. E. & d'Auria, F. (1998), Computation of shock waves in cavitating flows, ASME/FED Third International Symposium on Numerical Methods for Multiphase Flow.

Colonius, T., d'Auria, F. & Brennen, C. (1999), 'Bubbly cavitating flow adjacent to an oscillating wall', *submitted to Physics of Fluids* pp. 1–33.

Delale, C. F., Schnerr, G. H. & Sauer, J. (1998), 'Quasi-one-dimensional cavitating nozzle flows. part 1. bubble/flow interactions', *unpublished* **1**, 1–38.

Hairer, E. & Wanner, G. (1996), *Solving Ordinary Differential Equations II*, rev edn, Springer.

Ishii, R., Umeda, Y., Murata, S. & Shishido, N. (1993), 'Bubbly flows through a converging-diverging nozzle', *Physics of Fluids A-Fluid Dynamics* **5**(7), 1630–1643.

Matsumoto, Y. & Kameda, M. (1996), 'Propagation of shock waves in dilute bubbly liquids', *JSME International Journal* **39**(2), 264–272.

Press, W. H., Teukolsky, S. A., Vettering, W. T. & Flannery, B. P. (1994), *Numerical Recipes in FORTRAN : the art of scientific computing*, 2nd edn, Cambridge University Press.

Sandhu, N. & Jameson, G. J. (1979), 'An experimental study of choked foam flows in a convergent-divergent nozzle', *International Journal of Multiphase Flow* **5**, 39–58.

Tangren, R. F., Dodge, C. H. & Seifert, H. (1949), 'Compressibility effects in two-phase flow', *Journal of Applied Physics* **20**(7), 637–645.

van Wijngaarden, L. (1968), 'On the equations of motion for mixtures of liquid and gas bubles', *Journal of Fluid Mechanics* **33**, 465–474.

van Wijngaarden, L. (1972), 'One-dimensional flow of liquids containing small gas bubbles', *Annual Review of Fluid Mechanics* **4**, 369–396.

Wang, Y.-C. (1996), Shock Waves in Bubbly Cavitating Flows, PhD thesis, California Institute of Technology.

Wang, Y.-C. (1999), Stability analysis of one-dimensionl steady cavitating nozzle flows with bubble size distribution, 1999 ASME/JSME FED Summer Meeting.

Wang, Y.-C. & Brennen, C. (1998), 'One-dimensional bubbly cavitating flows through a converging-diverging nozzle', *Journal of Fluids Engineering-Transactions of the ASME* **120**(1), 166–170.